

## Supplementary Appendix

This appendix has been provided by the authors to give readers additional information about their work.

Supplement to: Babenko AP, Polak M, Cavé H, et al. Activating mutations in the *ABCC8* gene in neonatal diabetes mellitus. *N Engl J Med* 2006;355:456-66.

## SUPPLEMENT

### Activating Mutations in *ABCC8* cause Neonatal Diabetes Mellitus

Andrey P. Babenko, M.D., Ph.D., Michel Polak, M.D., Ph.D., H el ene Cav e, D.Pharm., Ph.D., Kanetee Busiah, M.D., Paul Czernichow, M.D., Raphael Scharfmann, Ph.D., Joseph Bryan, Ph.D., Lydia Aguilar-Bryan M.D., Ph.D., Martine Vaxillaire, D.Pharm., Ph.D., and Philippe Froguel, M.D., Ph.D.

#### **METHODS**

Between 06/1995 and 06/2005, 73 patients with neonatal diabetes were referred to the French network for the study of neonatal diabetes mellitus for genetic diagnosis. This network began as a retrospective study and has evolved into a prospective multi-center effort. Patients were recruited on a voluntary basis through a network of physicians involved in the treatment of diabetes mellitus.<sup>1</sup>

#### **Sequencing**

Genomic DNA was amplified by PCR with primers designed to cover all 39 exons and flanking intron-exon boundaries of the *ABCC8* gene. The PCR products were purified using Multiscreen® PCRµ96 plates (Millipore, Billerica, MA) and directly sequenced by double-stranded DNA cycle sequencing (Applied Biosystems, Foster City, CA) according to the manufacturer's instructions. The identity of mutations was confirmed on each sample by re-sequencing using the original genomic DNA. All of the nucleotide sequence analysis was verified by two independent examiners.

## **Molecular Biology**

Mutations for the analysis of ND channels were introduced into hamster SUR1 cDNA<sup>2</sup> using the Quik-Change mutagenesis protocol (Stratagene, Inc, La Jolla, CA). All the mutated residues are conserved in hamster vs human SUR1, based on a ClustalX alignment of mammalian ABCC8 proteins; the human numbering is used throughout (sequence files Q09428 and L40623 for human and hamster *ABCC8* are available in the Swiss-Prot and NCBI databases, respectively). Individual mutations were verified by sequencing.

## **Electrophysiological Analysis**

Patch-clamp recordings and  $K_{ATP}$  channel current analyses were done as described previously.<sup>3,4</sup> The activity of the  $N$  identical channels with the mean open channel probability  $P_O$  is  $N \cdot P_O = I/i$ , where  $I$  is the mean current through all  $K_{ATP}$  channels in the patch and  $i$  is the single-channel current amplitude at a given  $K^+$  driving force. Transfected COSm6 cells have negligible endogenous  $K^+$  and other ATP-dependent background currents and allow a unambiguous determination of the zero  $K_{ATP}$  current-level (shown as a dotted line in Figures S2, S4, and S5) and thus accurate measurement of virtually any low  $I$ . The inwardly directed  $K_{ATP}$  currents (downward deviations of traces in Figures S2, S4, and S5) were recorded using symmetrical  $K^+$ -rich pipette and bath solutions and the holding potential of  $-40$  mV in both cell-attached (on-cell) and inside-out configurations. None of the mutations in SUR1 affected  $i$  or made  $i$  for the inwardly directed currents sensitive to Mg, nucleotides, or sulfonylureas; the single-channel slope conductance around  $-40$  mV, determined as described previously,<sup>4</sup> was  $75 \pm 2$ ,  $73 \pm 3$ , and  $74 \pm 2$  pS for the I1424V, H1023Y, and WT channels in 6, 6, and 6 experiments, respectively. The symmetrical  $K^+$ -rich solutions essentially zeroed any intrinsic potential of COSm6 cells with a large number of the exogenously expressed  $K^+$  channels,<sup>3,4</sup> nullifying any difference between

the holding potential and the  $K^+$  driving force in the cell-attached mode. Therefore  $i$  remained constant in both on-cell and inside-out configurations during recordings from large macropopulations of recombinant channels (see, for example, the three lower traces in Figure S2). For every patch with a relatively small  $N$  (see, for example, the top trace in Figure S2), the  $i$  value on-cell was verified from an all-points current amplitude histogram. Thus  $I_{\div i}$  at any time in an analyzed record gave the mean activity of  $N$  identical channels,  $N \cdot P_O$ , and changes in  $I_{\div i}$  at constant  $N$  reflected changes in the mean  $P_O$ . The  $I_{\div i}$  values for each test solution and configuration were normalized to the ligand-independent  $I_{\max \div i}$  value for the same patch. The resulting fractions of the maximal activity from a number of cells ( $n > 5$ ) with each type  $K_{ATP}$  channels were expressed as a mean  $\% \pm SE$  in Figure 2. To approximate the heterozygous condition, cells were transfected with mutant and WT SUR1 (1:1 plasmid ratio) plus  $K_{IR6.2}$ . In the resulting heterogeneous population, the  $N \cdot P_O$  for each of the four expected sub-populations of structurally different hybrid mutant:WT SUR1 channels cannot be determined experimentally without *assuming* a defined distribution of channel subtypes and their single-channel properties, therefore only fractions of the *average* mean  $N \cdot P_{O_{\max}}$  for a heterogeneous population of channels are reported in the bottom panel in Figure 2. In all cases the differences in  $\%$  values with  $P < 0.05$  (unpaired t-test) were considered significant. To compare the responses of different channels to physiologic nucleotide conditions,  $I_{\div i}$  values were determined for the same channels in cell-attached and inside-out mode immediately after patch isolation and normalized to their maximal ligand-independent activity. To correct the ligand responses of isolated channels for inactivation and/or MgATP-dependent refreshment, their currents in the presence of test ligand(s) in the inside-out configuration were normalized to the arithmetic mean of their currents before rapid application of nucleotide(s) or drugs and after washout. The  $IC_{50(ATP)}$  values were determined by

fitting a pseudo-Hill equation to the steady-state ATP dose-response data.<sup>5</sup> The sulfonylurea sensitivity of mutant channels was determined by direct application of tolbutamide (Tlb), a first generation hypoglycemic agent, which was used here in preference to glibenclamide, a second generation hypoglycemic agent with higher affinity for SUR1, because its action on  $K_{ATP}$  channels is readily reversible thus facilitating comparison of currents before sulfonylurea binding and after washout.<sup>3</sup>

## RESULTS

### Mutations in SUR1 Map to Key Functional Domains

SUR1 is a member of the ATP-binding cassette (ABC) superfamily with a conserved core consisting of two transmembrane helical domains (TMD1 and 2), extended helical intracellular coupling domains (ICD1 and 2), and nucleotide-binding domains (NBD1 and 2) plus an additional amino terminal “gatekeeper” module,<sup>6</sup> TMD0-L0 (see supplementary Figure S1). The L213R mutation is in the intracellular region that links the transmembrane domain with the gatekeeper module, and thereby controls the channel  $P_{Omax}$ .<sup>6,7</sup> I1424V is in NBD2, the domain believed to hydrolyze MgATP.<sup>8</sup> It is also one amino acid away from the highly conserved Q1426 residue that defines the ‘Q-loop’; conformational transitions in this loop have been suggested to couple structural changes, as a result of nucleotide binding, with movements of TMD1 and TMD2.<sup>7,9</sup> H1023Y is in the first transmembrane helix of TMD2, which positions NBD2. The R1379C mutation lies within a particular sequence motif of NBD2, suggesting that it may alter ATP coordination. R1182Q is at the top of ICD2, which connects TMD2 with NBD2. Finally, C435R and L582V are in the third and last helices of TMD1, respectively. Based on the known structures<sup>10,11</sup> and biochemical characteristics of other transporters in the ABC superfamily, the orientation(s) of all of the TM and IC domains are expected to change with nucleotide-driven

dimerization of the NBDs, and may thereby stimulate the  $K_{ATP}$  pore via the “gatekeeper” module.<sup>6,7</sup>

## References

1. Metz C, Cave H, Bertrand AM, et al. Neonatal diabetes mellitus: chromosomal analysis in transient and permanent cases. *J Pediatr* 2002; 141:483-9.
2. Aguilar-Bryan L, Nichols CG, Wechsler SW, et al. Cloning of the beta cell high-affinity sulfonylurea receptor: a regulator of insulin secretion. *Science* 1995; 268:423-426.
3. Babenko AP, Gonzalez G, Bryan J. The tolbutamide site of SUR1 and a mechanism for its functional coupling to  $K_{ATP}$  channel closure. *FEBS Lett* 1999; 459:367-76.
4. Babenko AP, Bryan J. A conserved inhibitory and differential stimulatory action of nucleotides on  $K_{IR6.0}/SUR$  complexes is essential for excitation-metabolism coupling by  $K_{ATP}$  channels. *J Biol Chem* 2001; 276:49083-92.
5. Babenko AP, Gonzalez G, Aguilar-Bryan L, Bryan J. Sulfonylurea receptors set the maximal open probability, ATP sensitivity and plasma membrane density of  $K_{ATP}$  channels. *FEBS Lett* 1999; 445:131-6.
6. Babenko AP, Bryan J. SUR domains that associate with and gate  $K_{ATP}$  pores define a novel gatekeeper. *J Biol Chem* 2003; 278:41577-80.
7. Babenko AP.  $K_{ATP}$  channels "vingt ans après": ATG to PDB to Mechanism. *J Mol Cell Cardiol* 2005; 39:79-98.
8. Matsuo M, Kioka N, Amachi T, Ueda K. ATP binding properties of the nucleotide-binding folds of SUR1. *J Biol Chem* 1999;274(52):37479-82.

9. Jones PM, George AM. Mechanism of ABC transporters: a molecular dynamics simulation of a well characterized nucleotide-binding subunit. *Proc Natl Acad Sci U S A* 2002;99(20):12639-44.
10. Chang G. Structure of MsbA from *Vibrio cholera*: a multidrug resistance ABC transporter homolog in a closed conformation. *J Mol Biol* 2003; 330:419-30.
11. Reyes CL, Chang G. Structure of the ABC transporter MsbA in complex with ADP, vanadate and lipopolysaccharide. *Science* 2005;308(5724):1028-31.
12. Ashfield R, Gribble FM, Ashcroft SJ, Ashcroft FM. Identification of the high-affinity tolbutamide site on the SUR1 subunit of the  $K_{ATP}$  channel. *Diabetes* 1999; 48:1341-7.

## FIGURE LEGENDS

### **Figure S1. PND and TND Mutations in SUR1 Map to Domains Expected to Undergo Mg-nucleotide-dependent Conformational Transitions.**

The residues mutated in PND and TND patients are shown as red and green spheres, respectively. Amino-acids are designated by their single-letter codes. TMD, ICD and NBD indicate transmembrane, intracellular coupling and nucleotide-binding domains, respectively. A homology model of the ‘relaxed’ human SUR1 core (see<sup>6</sup> and its supplement) based on the VC-MsbA coordinates<sup>10</sup> is shown in conventional ribbon diagram format. The TMD1-ICD1-NBD1 and TMD2-ICD2-NBD2 halves of the core are in gray and blue, respectively. SU indicates the position of Ser1237 important for selective interactions of tolbutamide with SUR1 vs SUR2A.<sup>12</sup> Loops that were built *de novo* are not displayed. No structural template for the N-terminal TMD0-L0 gatekeeper module is available and the cartoon is based on previous computational analysis.<sup>7</sup>

**Figure S2. Representative Current Records from COSm6 Cells Transfected with Mutant and/or Wild Type SUR1 Subunit(s) plus K<sub>IR</sub>6.2.**

Records are from the same population of channels ‘on-cell’ and in inside-out configuration in the presence of 1 mM ATP, with or without Mg<sup>2+</sup>, as indicated by the horizontal bars. An arrow marks the time of membrane patch excision. The dotted lines show the zero current levels. The holding potential was –40 mV. The pipette solution contained (in mM): KCl, 145; MgCl<sub>2</sub>, 1; CaCl<sub>2</sub>, 1; HEPES, 10; pH 7.4 (KOH). The Mg<sup>2+</sup>-free bath solution contained (in mM): KCl, 140; EDTA, 5; HEPES, 5; KOH, 10; pH 7.2 (KOH). The bath “intracellular” solution contained (in mM): KCl, 140; MgCl<sub>2</sub>, 1; EGTA, 5; HEPES, 5; KOH, 10; pH 7.2 (KOH). The free Mg<sup>2+</sup> concentration, [Mg<sup>2+</sup>]<sub>i</sub>, in nucleotide-containing solutions was kept at a quasi-cytosolic level of ~0.7 mM by adding MgCl<sub>2</sub>. The scale bars give the time (10 seconds) and indicated current values. The colors in all Figures are keyed to Figure S1.

**Figure S3. The ATP Dose Response of H1023Y- vs WT-SUR1 Containing K<sub>ATP</sub> Channels in the Presence of ~0.7 mM free Mg<sup>2+</sup>.**

The activity values (mean±SE) obtained from 6 ND vs 6 control inside-out patches are shown. The data overlap at low, non-physiologic concentrations of Mg-ATP (~0.01 mM), but the activity of the ND channels is significantly higher when Mg-ATP is ≥0.1 mM. The data points are interpolated by a spline curve for illustrative purposes.

**Figure S4. Similar Spontaneous Activity of ND vs WT K<sub>ATP</sub> Channels is Similarly Inhibited by ATP.**

Segments of representative current records from inside-out patches from COSm6 cells transfected with K<sub>IR</sub>6.2 plus the indicated regulatory subunit. The thick and thin horizontal bars

indicate the application of 1 mM and 10  $\mu$ M ATP, respectively, in the absence of  $Mg^{2+}$ . All time bars show 10 s; all current bars show 0.1 nA.

**Figure S5. Sulfonyleurea Sensitivity of I1424V and H1023Y Channels.**

Representative current records from inside-out patches from COSm6 cells transfected with  $K_{IR6.2}$  plus the indicated receptor in Mg-free internal solution (Panel A) and in the presence of Mg-nucleotides (Panel B). The horizontal bars indicating the application of different ligands are defined once for all traces. Tlb, tolbutamide. All time bars show 10 s; all current bars show 0.1 nA.

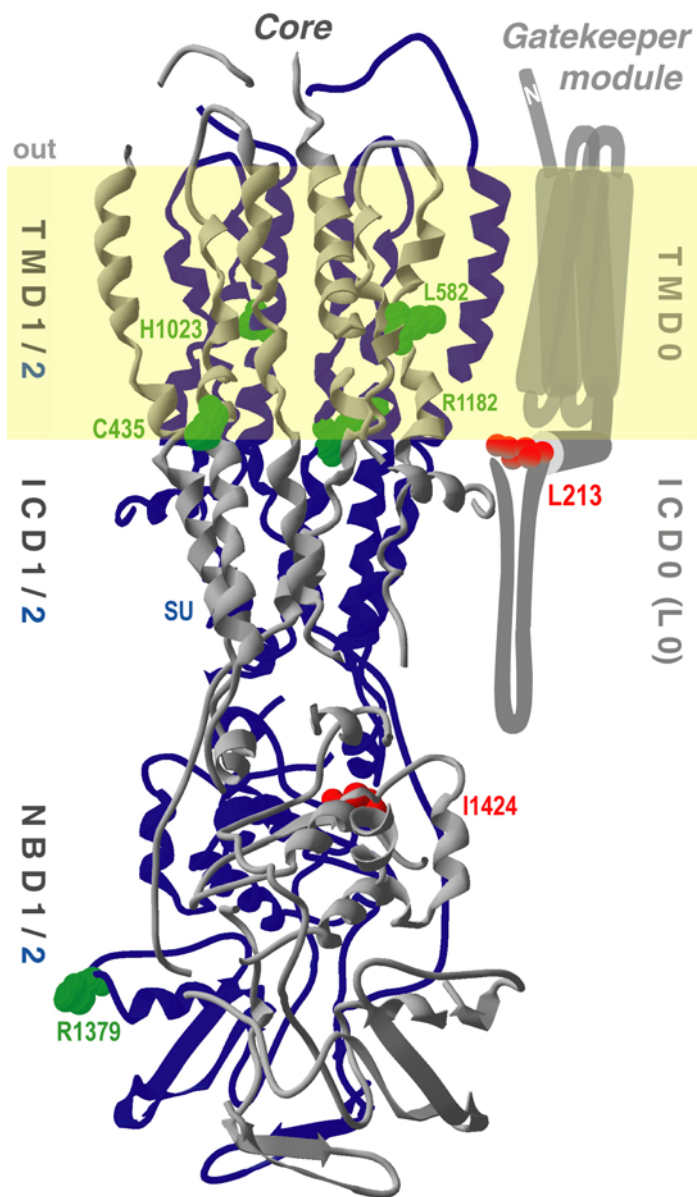


**Figure S1**  
 Babenko et al., 2006  
*Activating mutations in...*

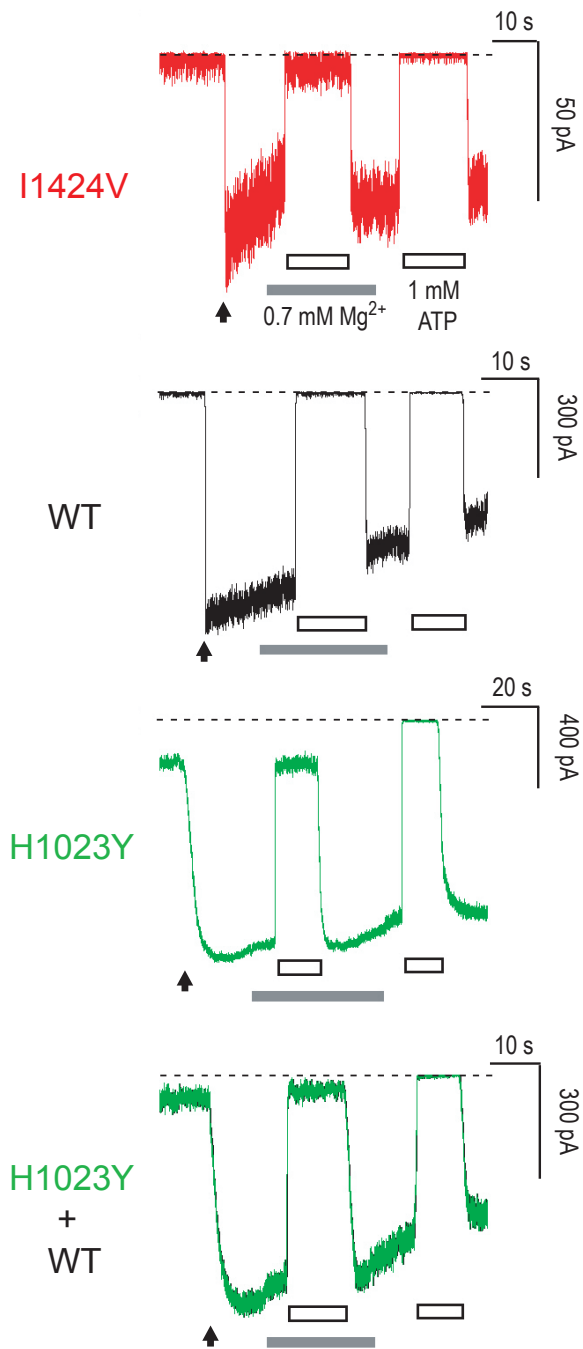


**Figure S2**  
 Babenko et al., 2006  
*Activating mutations in...*

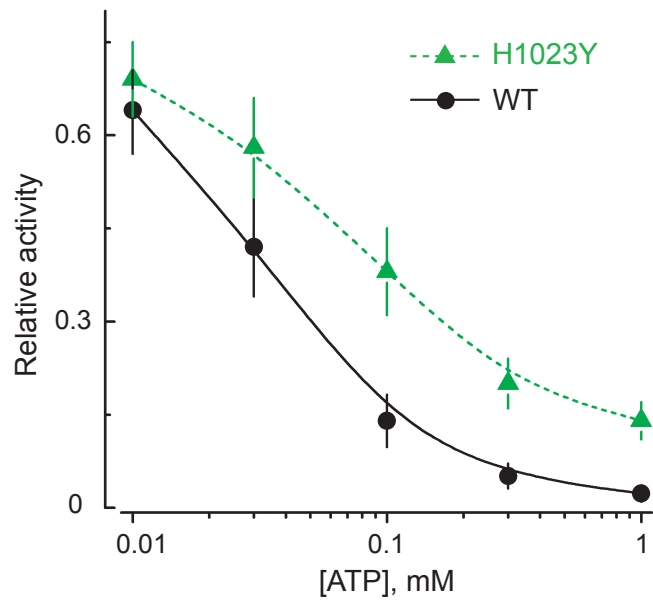


**Figure S3**  
Babenko et al., 2006  
*Activating mutations in...*

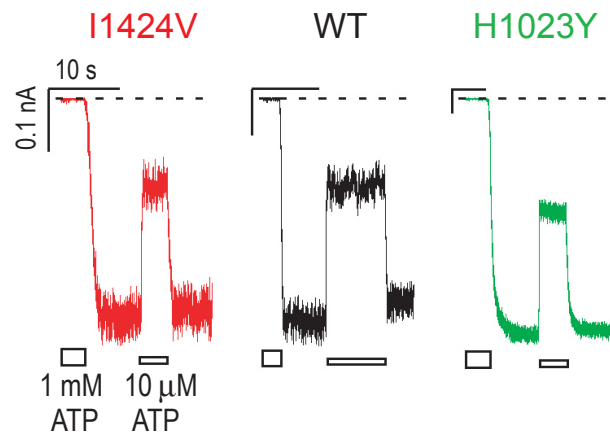


**Figure S4**  
Babenko et al., 2006  
*Activating mutations in...*

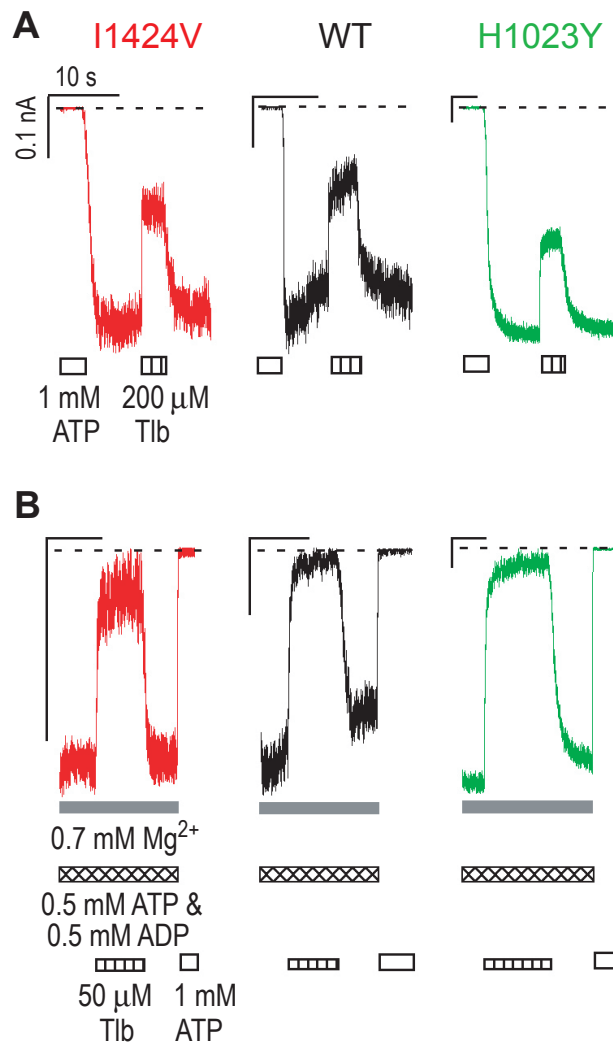


**Figure S5**  
 Babenko et al., 2006  
*Activating mutations in...*

**Table S1. Comparison of Clinical Features\* of ND Patients with Mutant *KCNJ11*, *ABCC8* or Abnormal 6q24.**

	<b>PND-KCNJ11 (n=12)</b>	<b>PND-ABCC8 (n=2)</b>	<b>TND-ABCC8 (n=7)</b>	<b>TND-6q24 (n=25)</b>
<b>GESTATION</b>				
Weeks	38.2(38-41)	40.5(40-41)	39.4(34-40)	36(36-41)
Weight (g)	2680.7(2110-3260)<3-60	3072(3065-3080)22-25	2795(1830-3570)<3-67	1830(1200-3570)<3-25
<b>AT DIAGNOSIS</b>				
Age (day)	57(1-127)	79(33-125)	29.9(3-74)	4(1-34)
Weight (g)	3681(2110-5040)	4340(3360-5320)	3594.2(1680-6100)	1894(1200-6100)
Glucose (mmol/liter)	37.5(9.5-55)	47.3(28.6-66)	34(6.9-51.4)	22(7.3-43.6)
% of patients with				
ketoacidosis	75	50	14	4
polyuria and polydipsia	8	50	57	8
glucose monitoring	17	0	29	88
Months of initial insulin therapy	Not applicable	Not applicable	4(1-10)	2.6(0-35)
% of patients with neurologic features				
developmental delay	25	50	0	12
seizures or epilepsy	8	0	0	0
dyspraxia	17	0	14	0

\*averaged characteristics are expressed as mean(range)percentile.

**Table S1**  
Babenko et al., 2006  
*Activating mutations in...*